CONTENTS

1. SUMMARY

In June 2000, two M=6.5 earthquakes occurred in the South Iceland Seismic Zone (SISZ) (Árnadóttir et al. 2001; Pedersen et al. 2001; Pedersen et al. 2003; Stefánsson et al. 2003; Clifton and Einarsson 2005). Following the earthquakes, seismicity greatly increased in all of southwestern Iceland. Roughly nineteen thousand microearthquakes, recorded by the SIL seismic network between June and December 2000 and interactively analyzed, have been relatively located using a multi-event relocation method. The procedure increases location accuracy to such a degree that fault patterns defined by the microearthquake distribution may become resolvable. Joint interpretation of the event distribution and focal mechanisms allows definition of common fault planes and the determination of slip directions on these faults. The mapped area includes the South Iceland Seismic Zone, the Reykjanes Peninsula (RP) and an area surrounding the Geysir geothermal system on the eastern margin of the Western Volcanic Zone (WVZ). The mapping reveals finer details of the faults which ruptured in the two M=6.5 events, and shows an interesting difference between their fault patterns. Numerous other smaller faults and clusters, which were illuminated by the increased activity, are also mapped. These mostly show the common northerly striking trend observed on the surface, with near vertical fault planes and right-lateral slip, accompanied by a vertical component. In some areas deviation from this trend is seen and westerly striking faults are observed, exhibiting left-lateral movement. The mapped events are shown in Figure 1.

2. INTRODUCTION AND METHOD

The relative relocation method takes advantage of the fact that seismic wave forms from microearthquakes occurring in a cluster are often very similar, especially if they originate on the same fault. If the inter-event distance is small compared to the distance from the cluster to a receiver, then the seismic ray paths from the events to the station will be almost the same and the small difference in travel time will be primarily due to the relatively short distance between the events. Cross-correlation of wave forms, both P and S, at each station is used to determine relative travel times of waves from the events to the station with sub-sample accuracy. The matrix of differences between these relative travel times and theoretical travel times is iteratively inverted to solve for the location by minimizing the time residuals (Slunga et al. 1995).

The mechanism of each event is obtained through a grid search (with a 4° angular interval) over all possible combinations of strike, dip and rake (Rögnvaldsson and Slunga 1994). The radiation pattern at each grid point is calculated and compared to the measured amplitudes at each station and first-motion polarities, where they have been specified. Only those solutions having amplitude error within certain limits and fulfilling the polarity requirements, with a few exceptions, are stored as possible fault-plane solutions for the event. Finally, joint interpretation of the event distribution with the focal mechanisms allows the determination of slip directions on common faults. Figures 2a and 2b show two examples of this joint interpretation. The faults are shown in both map view (left) and vertical view (right) perpendicular to strike. The optimal fault plane solution for each event is the one which best fits the strike and dip of the common fault. It is represented by a disk, which is scaled to the event's magnitude. The direction of slip is indicated by a tick mark on each circle. The figures

show that the best fault plane solutions are fairly close to the strike and dip of the overall fault planes. Furthermore, the slip directions of the events are fairly consistent on both faults, showing predominantly right-lateral slip.

The relocation software, which has been under constant development since 1999, had not been rigorously tested. Therefore extensive tests were performed to determine its robustness and reliability, as well as the reliability of the data. A summary of these tests can be found in the PREPARED first periodic report (Hjaltadóttir and Vogfjörð 2004). In general these tests showed the method to be reliable and stable.

The area under study encompasses southwestern Iceland, from the Reykjanes Peninsula (RP) through the South Iceland Seismic Zone (SISZ), with the addition of the area surrounding the Geysir geothermal system at the eastern edge of the Western Volcanic Zone (WVZ). The regions were divided into fifteen boxes, marked A-O in Figure 1, according to clustering of activity and the maximum number of 1800 events allowed in each box. The hypocenters of the two M=6.5 events, occuring on June 17th (J17) and 21st (J21), are marked as large green stars in boxes N and O, respectively. The J17 event triggered four additional events of magnitude around five. The hypocenters of these are marked by smaller green stars in Figure 1.

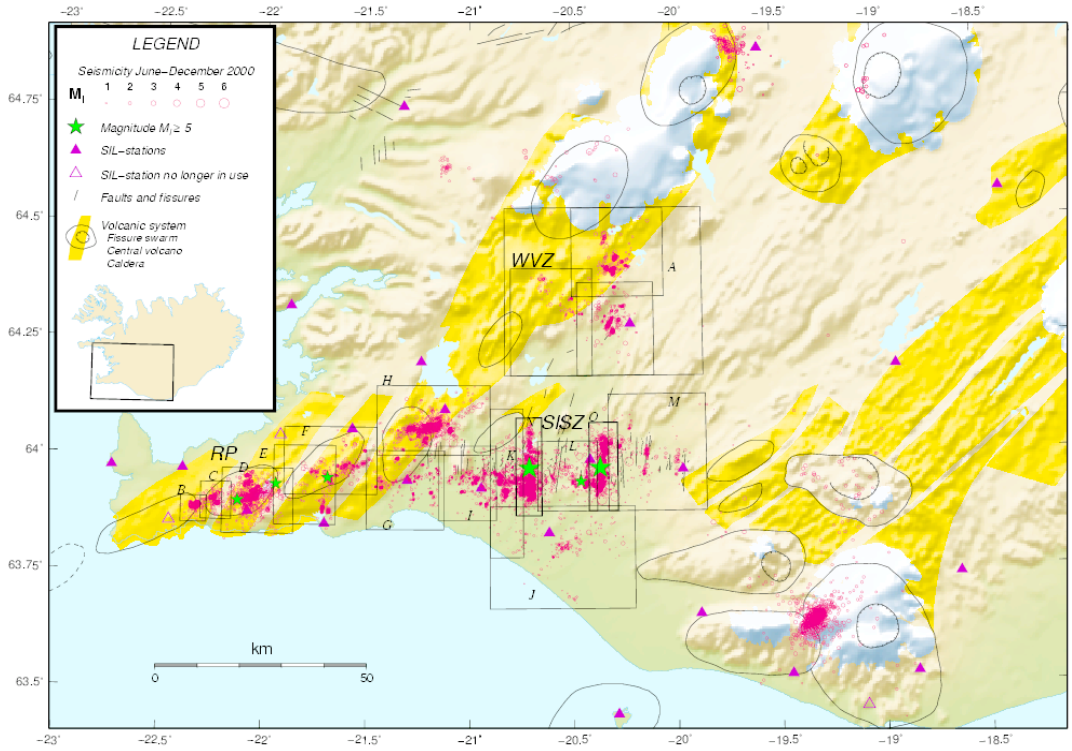

Figure 1. *Map of southwestern Iceland showing the aftershock activity in June-December following the two M=6.5 earthquakes on June 17th and June 21st. Their hypocenters are plotted as large green stars in boxes O and N respectively. The four smaller green stars show the hypocenters of four M~5 earthquakes, triggered by the J17 event. The study area was divided into fifteen boxes, outlined on the map and marked by A-O, for analysis. Roughly half of the nineteen thousand events displayed here, occurred outside the two main faults. Black lines denote mapped surface faults (Einarsson et al. 2005). Main tectonic features are also shown (Einarsson and Sæmundsson 1987).*

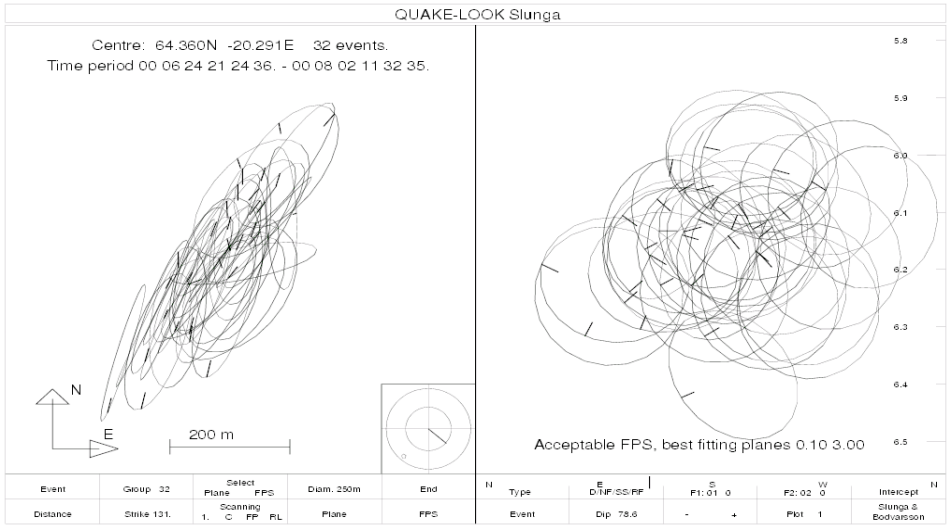

a)

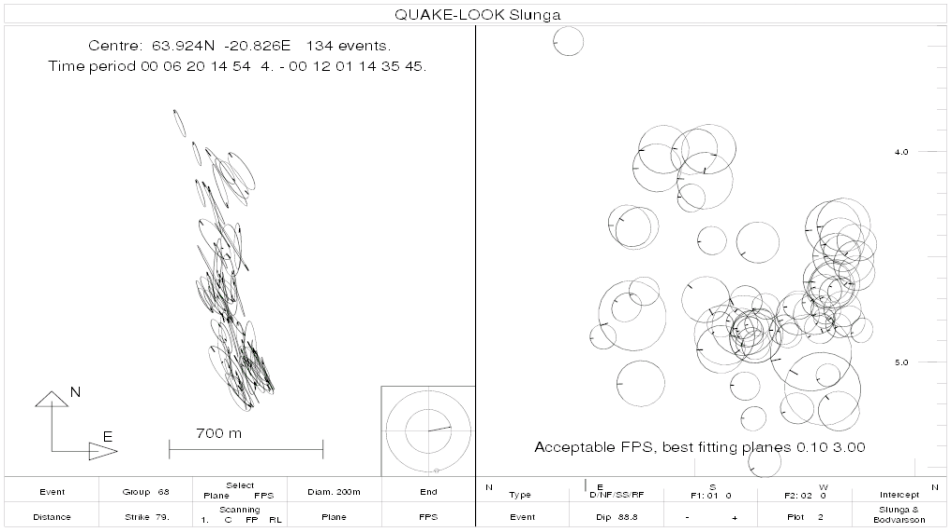

b)

Figure 2. *Joint interpretation of event distributions and focal mechanisms. a) Fault 3 in Figure 9a (box A02) in map view (left) and vertical view (right) perpendicular to strike; the angle of view is shown in the small boxed circle. Each earthquake is represented by a disk which is oriented according to the focal mechanism that best fits the strike and dip of the common fault plane. Furthermore, the size of the disk is scaled according to the event's magnitude and the tick mark indicates the direction of slip. The western block is moving to the left and slightly downwards, indicating an overall right-lateral motion with a smaller normal component. b) Same scheme as in a). This fault segment is located in box K in the SISZ (Figure 1). The tick marks indicate a predominant right-lateral motion on this northwards striking fault.*

3. RESULTS

3.1 June 2000 faults

3.1.1 June 17 fault

The June 17th fault is roughly 12.5 km long and 10 km deep. Aftershocks on the fault are mainly confined to the fault margins, mostly below 3 km, and a cluster in the center of the fault, around the hypocenter (Figure 3). During the first 24 hours, however, aftershocks were distributed over the entire fault. The fault is near vertical, with overall strike ~7°, but it is composed of many smaller sections with differing strikes.

Above 8 km depth the aftershocks display a rather discontinuous pattern composed of three main patches, each approximately 2-3.5 km long (Figure 4). The central patch is very planar and was active throughout the year. Its strike (~11°) is slightly east of the overall strike of the fault. Activity on the northernmost fault section is mostly near its northern edge, where it branches into a few short N-striking planes. The southernmost section is more continuous and bends westwards with decreasing latitude. At the southern tip the fault jumps half a kilometer to the west and continues on a ~2 km long segment. West of the southern edge, a few small faults were also activated. Their strikes are generally west of north.

Below 8 km depth the aftershocks define a continuous fault trace, but with kinks at the intersections of the main sections above. Below the northernmost fault section, the bottom appears to be composed of a few smaller en-echelon faults and then breaks up into separate parallel branches farther north. Activity on the southernmost fault patch, on the other hand, appears to be continuous and more linear, bending slightly westward towards the southern end.

Fault plane solutions of the events at the bottom of the fault predominantly show right-lateral, normal motion, whilst events in the center have a small thrust component added to the dominant right-lateral slip.

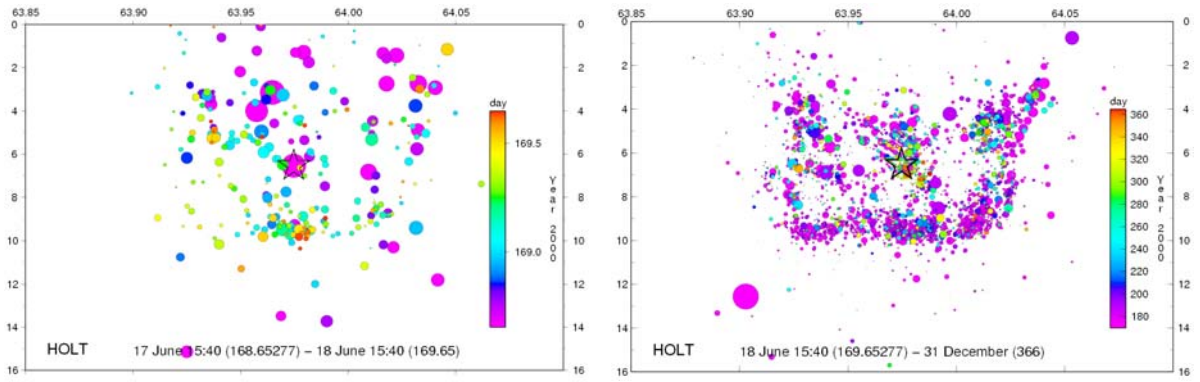

Figure 3. *Aftershocks on the J17-fault colour coded according to age. Left: the first 24 hours showing activity distributed across the entire fault. Right: Aftershocks after the first 24 hours and throughout the year showing activity mostly confined to the edges and the central patch near the hypocenter, here marked by a star.*

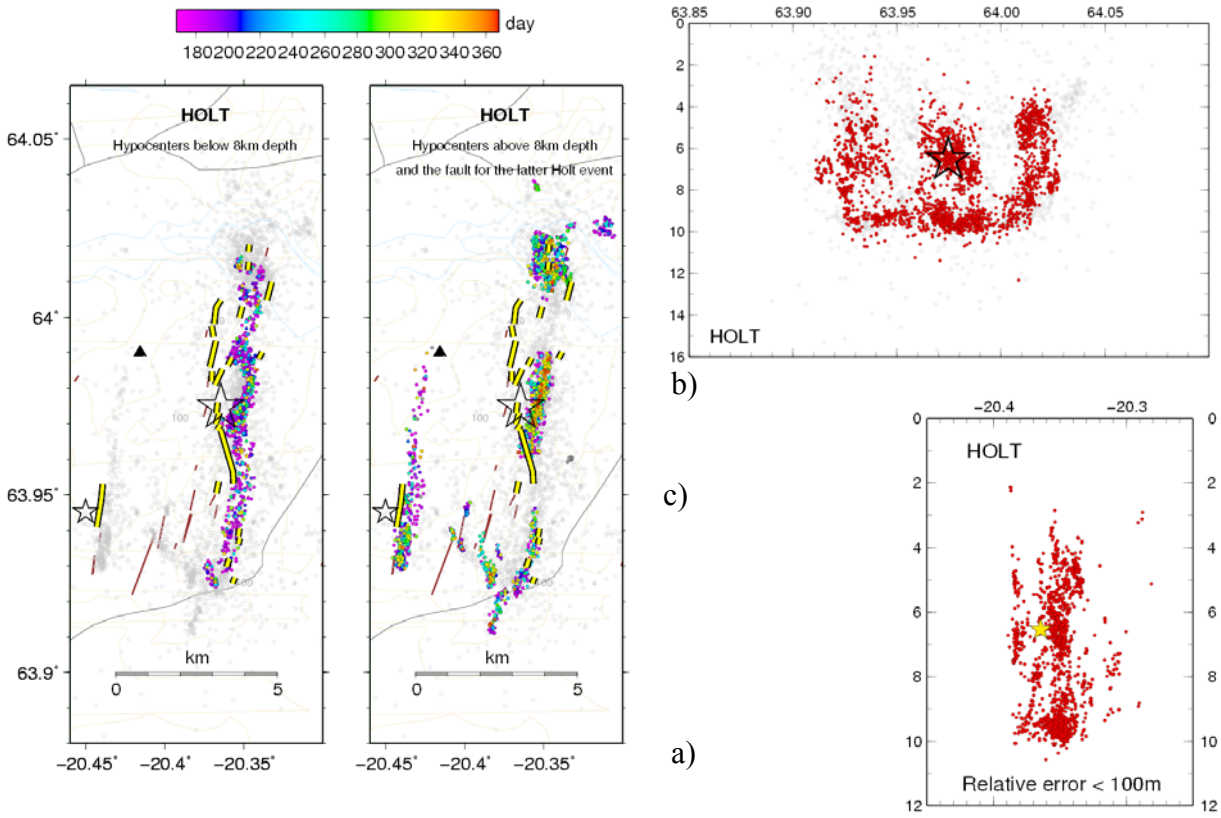

Figure 4. *Aftershocks on the Holt fault. a) Map view with all events shown in the background in grey. Events on identified faults are colour coded according to age (from June 17th to December 31st). The hypocenter of the main event is shown as a star. The star on the smaller fault, 5 km west of the J17 fault, marks the hypocenter of the second Holt event (M~5), occurring 2 minutes later. Events below 8 km depth are shown on the left; above 8 km on the right. Events on the second Holt fault, however, even though reaching 9.2 km depth, are all shown on the right. Mapped surface faults are displayed as yellow lines (Clifton and Einarsson 2005), brown lines denote older surface faults. b) Vertical view from east with coloured events from a) shown in red. c) Vertical view from south showing selected events (i.e. relative-error median <100 m).*

3.1.2 June 21 fault

During the time period between the two main shocks (June 17th to 21st), seismic activity in the epicentral area of the June 21st fault was mainly along the bottom of the eventual fault and along the trace of the mapped conjugate surface faults at ~63.95°, extending westward from the main fault (Figure 5). Additionally, seismicity also occurred along a second N-S lineament, located 2 km east of the main fault (at approximately -21.66°E). During the first 24 hours following the June 21st event, the aftershocks were distributed over the entire main fault up to about 1 km depth (Figure 6). After that, activity concentrated along the bottom, except at the southern end, where it was distributed over the whole depth range and continued throughout the year. South of the hypocenter, aftershocks are therefore evenly distributed over the fault, while north of the hypocenter the activity is sparser and mostly concentrated near the bottom. The overall fault length, defined by the aftershocks, is 16.5 km and its strike is 179°. The fault depth increases southward, from ~7 km on the northern half to ~10 km at the southern margin (Figure 7b).

Near the hypocenter the fault branches into two fault sections with different dips. The southern half is vertical and extends north to latitude 64°, terminating at the southern shore of lake Hestvatn (Figure 7a). The northern half dips 77° east and extends from the hypocenter to the northern margin of the fault, at 64.05°N. Both branches have the same northerly strike and follow approximately the same trace at the bottom, creating an approximately 3 km long wedge north of the hypocenter. The intersection of the dipping segment with the surface, approximately matches the mapped surface ruptures west of lake Hestvatn (Figure 7a). At the southern terminus, the fault is broken up into many small fault segments of 1-2 km diameter and with varying strike.

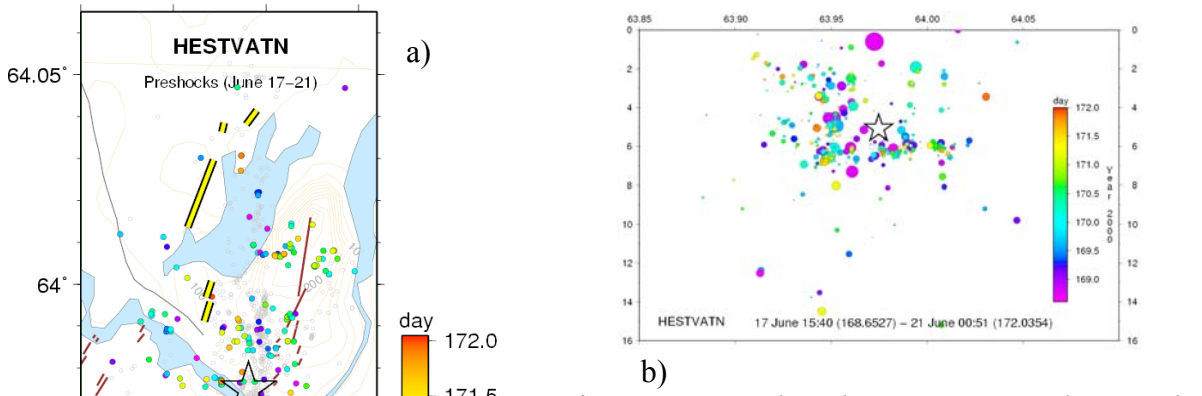

Figure 5. *Earthquakes occurring during the period between the two main shocks, from 15:40 UTC on June 17th to 00:51 UTC on June 21st, colour coded according to age. a) Map view showing seismicity concentrated 2 km south of the epicenter (indicated by a star) and westward along the trace of mapped surface faults (yellow lines; Clifton and Einarsson 2005). The trace of a second N-S fault, 2 km east of the J21 fault is also apparent. b) Vertical view from the east showing seismicity also concentrated along the bottom of the eventual fault.*

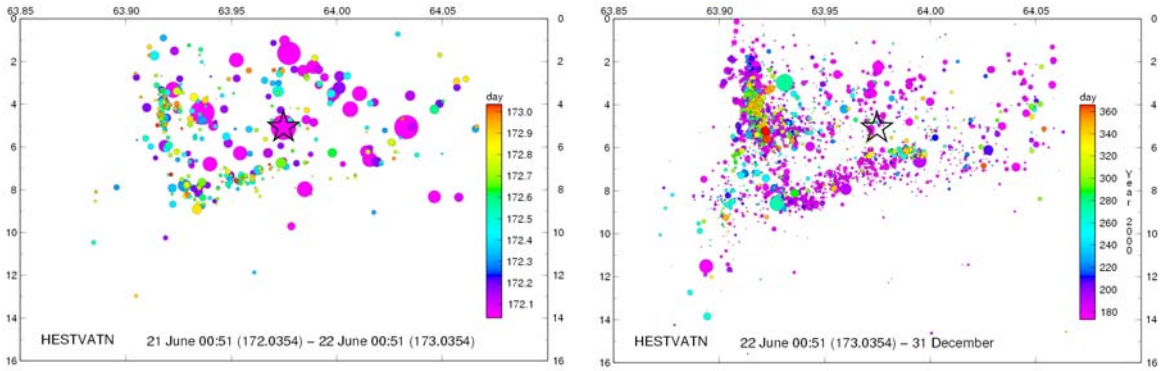

Figure 6. *Aftershocks on the J21 fault colour coded according to age. Left: the first 24 hours showing activity distributed across the entire fault, similar to the J17 fault. Right: Aftershocks after the first 24 hours and throughout the year showing activity mostly confined to the*

bottom and the southern end. The hypocenter is marked by a star.

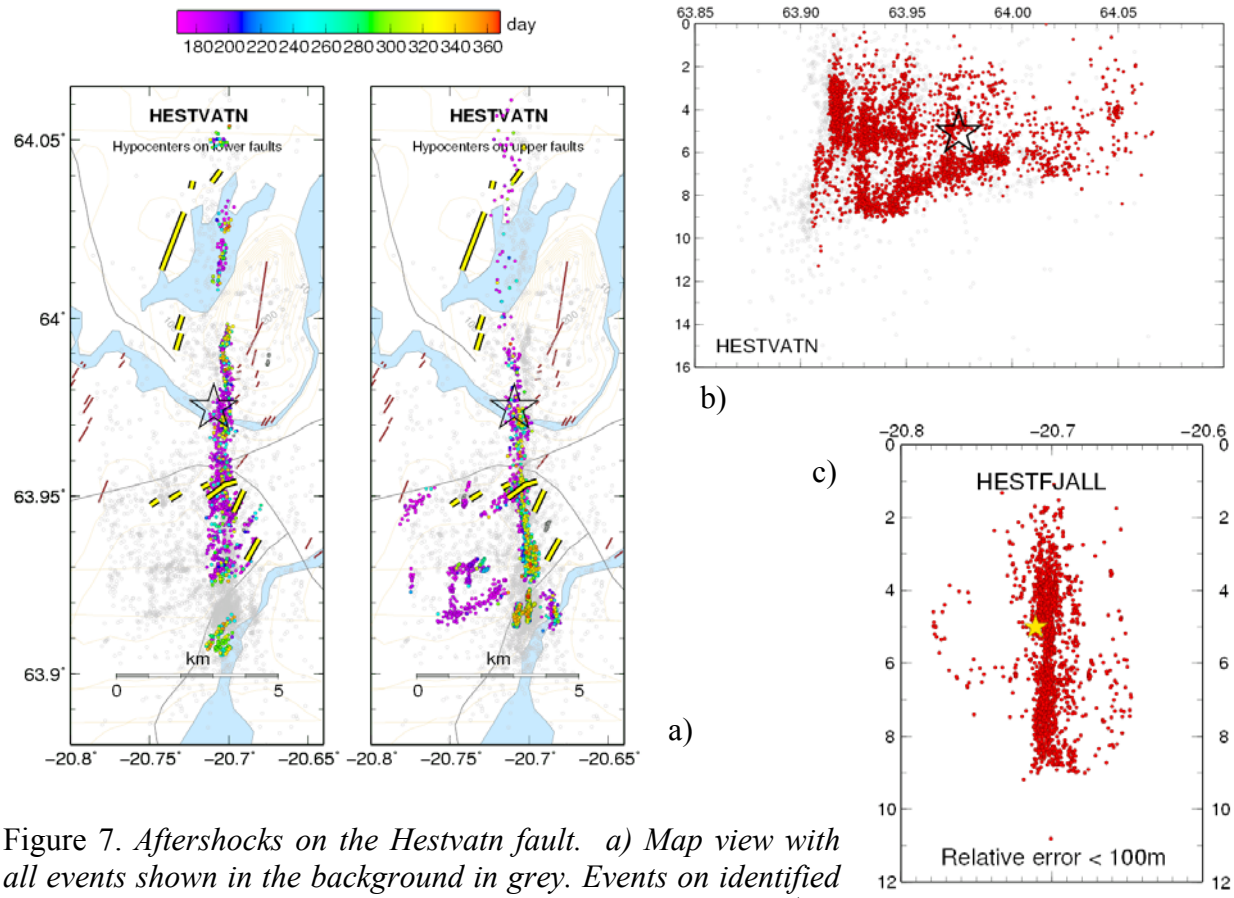

Figure 7. *Aftershocks on the Hestvatn fault. a) Map view with all events shown in the background in grey. Events on identified faults are colour coded according to age (from June 21st to December 31st). The hypocenter of the main event is shown as a star. Events along the bottom and below 6-7 km depth are shown on the left; above ~6 km on the right. Events on the E-W conjugate fault, however, even though reaching ~9 km depth, are all shown on the right. Mapped surface faults are displayed as yellow lines (Clifton and Einarsson 2005), brown lines denote older surface faults. b) Vertical view from east with coloured events from a) shown in red depicting the southward deepening of the fault. c) Vertical view from south showing selected events (i.e. relative-error median <100 m). A faint trace of the dipping wedge can be seen extending upwards and westwards from the hypocenter.*

Near the location of the mapped conjugate surface-rupture (Figure 7a), the earthquake distribution is denser and extends westward, mostly on short easterly striking segments. About 3 km farther south, a second set of conjugate faults, extending over a wide depth range (2-9 km) is also defined by the seismicity.

Slip directions on the southern end of the fault show predominantly right-lateral motion, with a slightly smaller normal component. Slip directions along the fault bottom are not as homogeneous having both thrust and normal components accompanying the dominant right-lateral motion, similar to the bottom layer of the Holt fault.

3.2 Other faults in Southwest Iceland

Innumerous smaller faults in Southwest Iceland were illuminated by the increased activity in 2000. Most of these strike close to north and show the predominant right-lateral motion, observed in the SISZ, accompanied by a normal component. In some areas, fault strikes deviate from the general trend, for example in the Hengill area (box H in Figure 1) and at Fagradalsfjall (box B), where E-W directions are also observed. These are predominantly left-lateral strike-slip faults, with a smaller normal component. Furthermore, north of the SISZ, at the eastern edge of the Western Volcanic Zone (box A), fault strikes are mostly NE-SW, similar to the dominant strike of the hyaloclastic ridges in the zone.

Distributed activity was observed on many of the large, historical faults in the SISZ (Figure 1). Although only separate segments on these were mapped, many of them can be linked with the aid of surface-fault maps (Einarsson et al. 2005). An example of mapped activity on an old fault can be seen in Figure 2b, which shows an approximately 1.5 km long fault section in the SISZ (box K in Figure 1). It appears to belong to a larger en-echelon fault, which most likely ruptured in a historical earthquake in 1734 (Páll Halldórsson, personal communication). The fault segment strikes 79°E, dips 87° and has a predominant right-lateral motion.

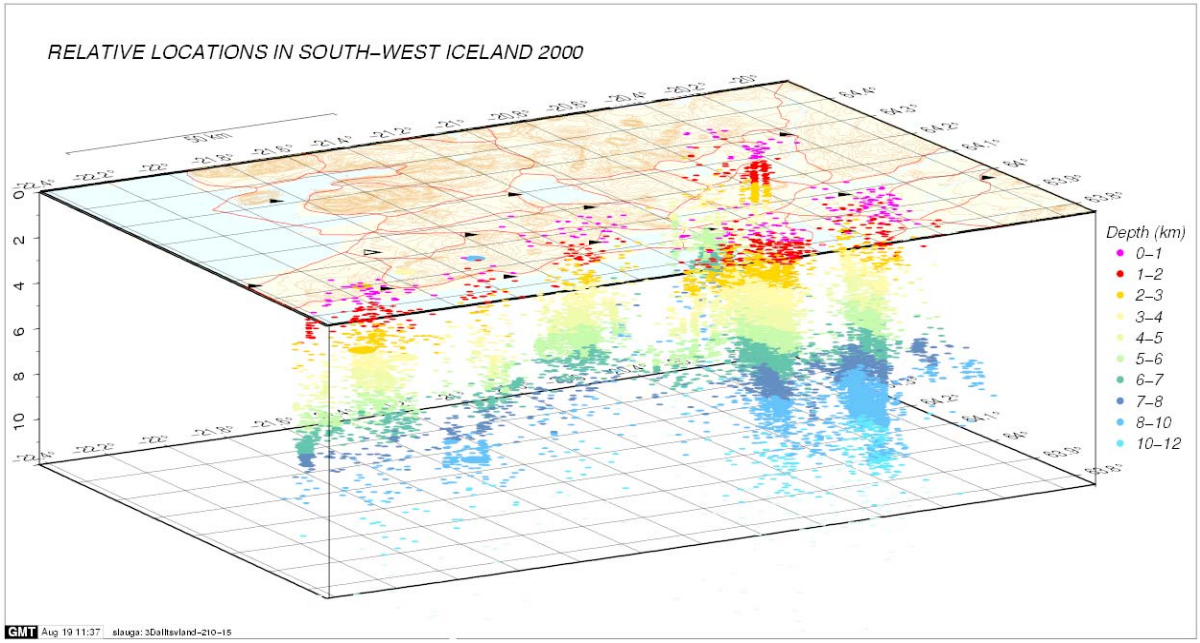

Figure 8. *A 3D-map showing all the relocated events. The hypocenters are colour coded according to their focal depth.*

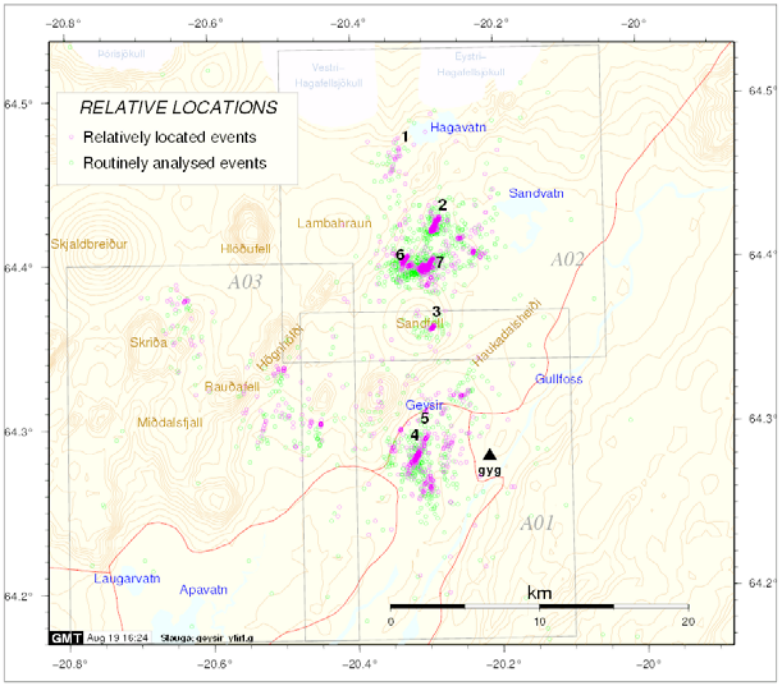

Figure 9a. *Overview of the Geysir area (box A in Figure 1). The area was divided into three sub-boxes, according to clustering of activity. Green circles show the single-event locations and the purple show relative locations.*

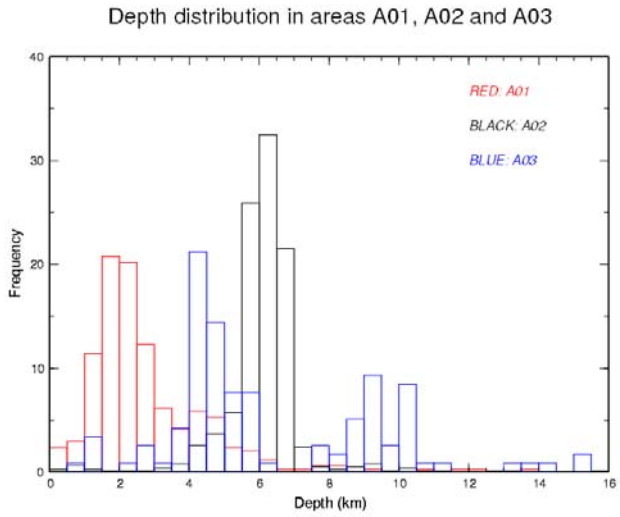

Figure 9b. *Histograms showing a different depth distribution in sub-boxes A01-A03, in the vicinity of the Geysir geothermal system. Shallower activity is observed in the nearest vicinity of the geothermal area (red).*

Figure 8 shows a 3D-map of all the relocated events colour coded according to focal depth. In general, earthquake activity extends to greater depths in the eastern part of SW Iceland than in the west. This may reflect the eastward thickening of the crust, from ~15 km in the RP to ~25 km in the eastern part of the SISZ, as revealed by refraction profiles (Weir et al. 2001; Vogfjörð et al. 2002) and tomography (Allen et al. 2002; Tryggvason et al. 2002). However, there is a deviation from this trend at the intersection of the WVZ and RP with the SISZ, in the center of the profile, were the maximum depth of seismicity reaches its shallowest level. This anomaly could be explained by volcanic activity in the Hengill volcanic system (box H in Figure 1). A second possibility is, that the discrepancy between the SIL velocity model, used in routine locations, and observed velocities in the RP (Weir et al. 2001; Vogfjörð et al. 2002) causes overestimation of source depths. The relocation method, however, should decrease errors caused by an incorrect velocity model.

A trend towards shallower activity is clearly observed in all geothermal regions, for example in the vicinity of the Krísuvík geothermal system (box D), in the Hengill (box H) and Geysir areas (box A). The overview map in Figure 9a shows both routine locations (green) and relative locations (purple) from the Geysir geothermal area. The relative locations are significantly better than the routine locations and most events line up on faults instead of the former fuzzy clusters. The fault labelled nr. 3, located under the shield volcano Sandfell, is the one shown in Figure 2a. It strikes SW, similar to most faults in the region, and dips 76°, which is sligthly less than the commonly observed 80°-90° dip. The motion on the fault is mainly right-lateral, with a smaller normal component. Box A was divided into three sub-boxes, A1-A3, according to the clustering of the activity, and the histograms in Figure 9b show the different depth distribution in the three sub-areas. The shallowest earthquakes occur in box A01, just south of the Geysir geothermal area, while farther north and west, in boxes A02 and A03, the activity is deeper.

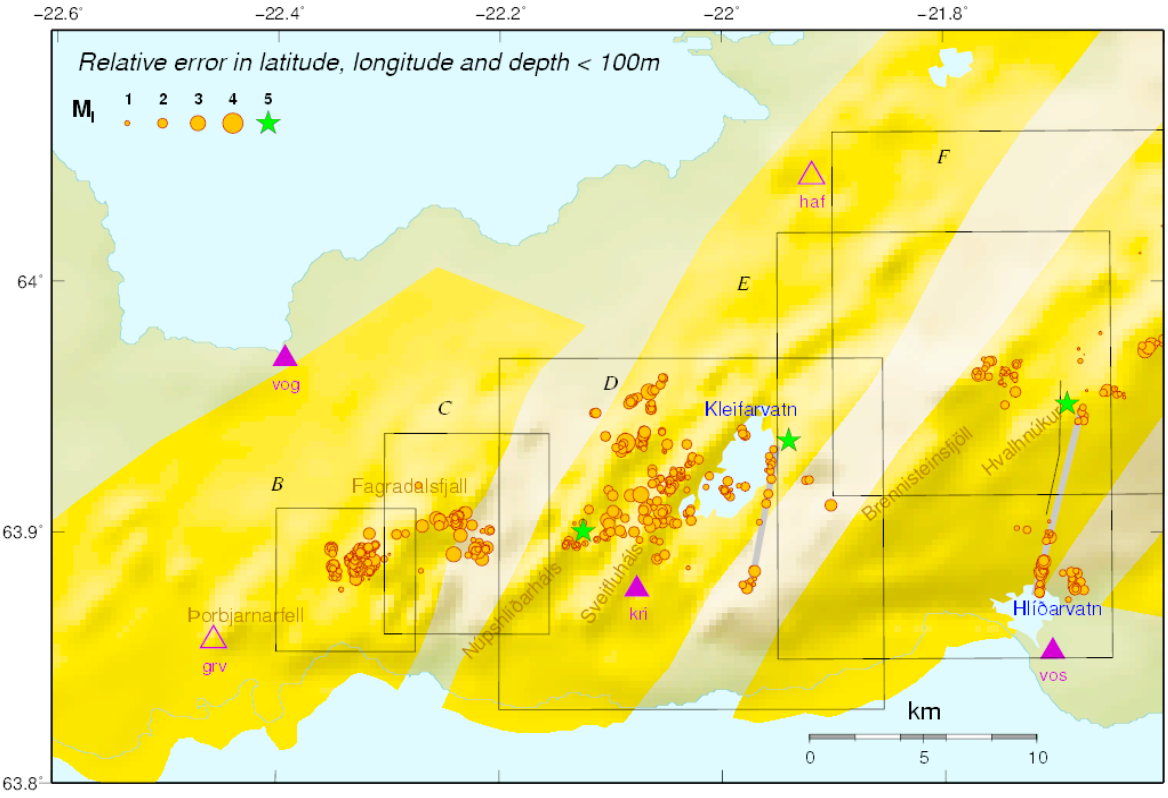

Figure 10. *Map of Reykjanes Peninsula. Earthquakes with relative-error median less than 100 m in latitude, longitude and depth are shown in orange, scaled according to magnitude. The hypocenters of the three triggered M~5 earthquakes on RP on June 17th are plotted as green stars. The thick gray line indicates approximate location of the fault planes for the Kleifarvatn and Hvalhnúkur events.*

Within minutes of the June 17th event, four M~5 events occurred; one near the south end of the J17 fault, the other three on RP (green stars in Figure 1) (Vogfjörð 2003; Clifton et al. 2003; Pagli et al. 2003). Two of these, the one in box F, near Hvalhnúkur, and the one near lake Kleifarvatn (box D), were dynamically triggered within the first 30 seconds by shear waves from the main event. The earthquakes' exact location and mechanism determination

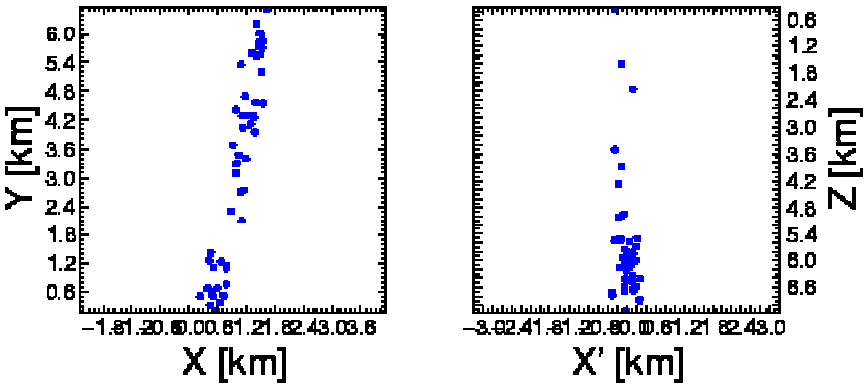

Figure 11. *Aftershocks mapped on the Kleifarvatn fault (box D in Figures 1 and 10). Left: the dimensions of the fault in map view. Right: vertical view along strike. The 50 events define a 6 km long, vertical fault plane.*

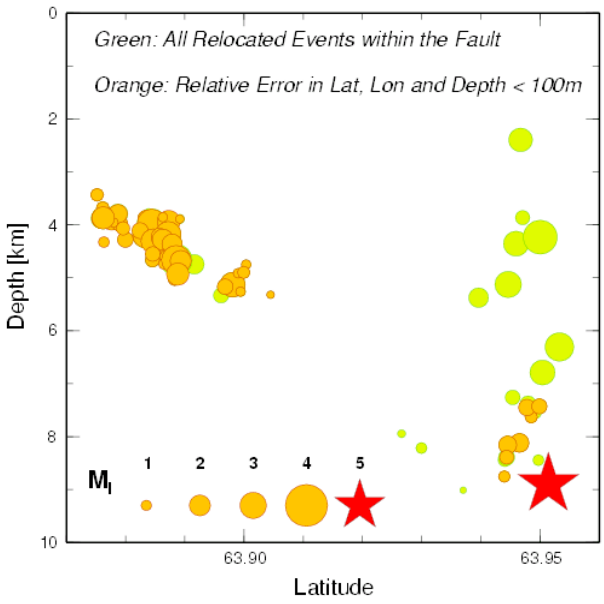

Figure 12. *A vertical view perpendicular to fault strike, showing the aftershocks defining the dimensions of the Hvalhnúkur fault. The hypocenters of all events are shown in green, while hypocenters with relative-error median less than 100 m in latitude, longitude and depth are shown on top in orange. The red star shows the hypocenter of the M~5 event at 9 km depth.*

have proven problematic because their waveforms are clipped and mixed in with the shear waves from the main event (Vogfjörð 2003; Antonioli et al. 2006). When relocated aftershocks with low relative error are extracted, as shown in Figure 10, indications of lineaments are revealed for both triggered events; one along the eastern shore of lake Kleifarvatn, the other north of lake Hlíðarvatn (shown as thick grey lines in Figure 10). In both cases the hypocenters are located at the northern tip of the fault planes. Figure 11 shows map view and vertical view along strike of the Kleifarvatn fault. The events lie on a 6 km long fault plane, with most of them occurring in the depth interval 5.4-6.8 km. The aftershock distribution on the Hvalhnúkur fault is even sparser than on the Kleifarvatn fault. Figure 12 shows a vertical view of the events perpendicular to fault strike. The hypocenter of the triggered event is at the bottom of the fault at approximately 9 km depth. The aftershocks at the northern end extend from the hypocentral depth up to 3 km. A clear fault is also seen at shallower depths (3.5-5.5 km) at the southern end. No events have yet been found between these two clusters. Though not contiguous, the aftershock distribution on the two faults provides valuable constraints on the fault areas and event magnitudes. The fault plane of the M~5 event, west of the J17 event, is well defined by the aftershock distribution (Figure 4a), but hardly any aftershocks were recorded on the fault plane of the westernmost M~5 event at Núpshlíðarháls.

4. DISCUSSION AND CONCLUSIONS

Using a double-difference relative relocation method to improve location accuracy of the aftershocks following the two M=6.5 June 2000 earthquakes, has revealed sub-surface fault patterns in Southwest Iceland, which have hitherto not been mapped. Many of the large historical faults in the SISZ experienced distributed activity, but generally not enough to map their outlines, since in most cases only small sections on each were activated. However, taking advantage of the surface mapping already performed (Clifton and Einarsson 2005) many can be inferred.

The mapping reveals the finer structural details of the two main faults, J17 and J21, and shows an interesting difference in character between the two. The Holt fault, of the J17 event, is approximately 12.5 km long and 10 km deep. It is nearly vertical, has an overall strike of 7°E and is broken up into three main sections, with each section striking a few degrees east of the overall fault strike. The trace of the 16.5 km long Hestfjall fault, on the other hand, is more linear, even though the fault is made up of two differently dipping sections. At the northern end the fault is about 7 km deep but deepens to 10 km at the southern end. Its strike is 179°E and the southern section dips ~88° to the west, while the dip on the northern section is 77°. Furthermore, large conjugate faults were active west of the J21 fault, extending as far as 2-3 km to the west. Both faults bend slightly westwards at their southern tip.

Many smaller faults in the SISZ, the RP and at the eastern margin of the WVZ have also been mapped. These show predominatly right-lateral motion on northerly or northeasterly striking faults, often accompanied by a smaller vertical component. However, a deviation from this trend is seen in some areas, where easterly striking faults with a left-lateral movement are also observed.

In general, maximum depth of seismicity increases from the RP, eastwards along the profile to the eastern SISZ. However, a deviation from this trend is observed in geothermal areas and in the middle of the profile, at the intersection of the RP, WVZ and SISZ, possibly caused by volcanic activity in the Hengill region.

Aftershock activity on the fault planes of the two S-wave triggered earthquakes on Reykjanes Peninsula has given valuable information for estimating the fault sizes of the two events. The earthquakes, which occurred within the first minute after the J17 event, were obscured and distorted by the previous event, making estimation of their size and mechanism problematic by other means.

5. ACKNOWLEDGEMENTS

This work is a part of the EC-funded project PREPARED (EVG1-CT-2002-00073). It was also funded by the Icelandic Graduate Student Research Fund (Rannsóknarnámssjóður).

All figures in this report, except for Figures 2a and 2b, were made with the GMT-software (Wessel and Smith 1991). See http://gmt.soest.hawaii.edu.

6. REFERENCES

Allen, R., G. Nolet, W.J. Morgan, K. Vogfjörð, M. Netles, G. Ekström, B.H. Bergsson, P. Erlendsson, G. Foulger, S.S. Jakobsdóttir, B. Julian, M. Pritchard, S. Ragnarsson and R. Stefánsson 2002. Plume driven plumbing and crustal formation in Iceland. *J. Geophys. Res*. 107 (B8), doi:101029/2001JB000584.

Antonioli, A., M.E. Belardinelli, A. Bizzarri and K.S. Vogfjörð 2006. Evidences of instantaneous dynamic triggering during the seismic sequence of year 2000 in South Iceland. *J. Geophys. Res.* 111 (in press).

Árnadóttir, Þ., S. Hreinsdóttir, G.B. Guðmundsson, P. Einarsson, M. Heinert and C. Völksen 2001. Crustal deformation measured by GPS in the South Iceland Seismic Zone due to two large earthquakes in June 2000. *Geophys. Res. Lett*. 28, 4031-4034.

Clifton, A.E., C. Pagli, J.F. Jónsdóttir, K. Eyþórsdóttir and K. Vogfjörð 2003. Surface effects of triggered fault slip on Reykjanes Peninsula, SW Iceland. *Tectonophysics* 369, 145-154.

Clifton, A.E. and P. Einarsson 2005. Styles of surface rupture accompanying the June 17 and 21, 2000 earthquakes in the South Iceland Seismic Zone. *Tectonophysics* 396, 141-159.

Einarsson, P. and K. Sæmundsson 1987. Earthquake epicenters 1982-1985 and volcanic systems in Iceland (map). In: Þ.I. Sigfússon (editor), *Í hlutarins eðli*. Festschrift for Þorbjörn Sigurgeirsson, Menningarsjóður, Reykjavík.

Einarsson, P., M. Khodayar, A.E. Clifton, B. Ófeigsson, S. Þorbjarnarson, B. Einarsson and Á.R. Hjartardóttir 2005. A map of Holocene fault structures in the South Iceland Seismic Zone. In: Abstracts from the EGU General Assembly, Vienna Austria, April 24-29, 2005. Abstract EGU05-A-08858.

Hjaltadóttir, S. and K.S. Vogfjörð 2004. WP5.1. Mapping subsurface faults in southwestern Iceland with the microearthquakes induced by the June 17th and June 21st earthquakes. In: PREPARED – first periodic report. *Icelandic Meteorological Office – Report* 04014.

Pagli, C., R. Pedersen, F. Sigmundsson and K.L. Feigl 2003. Triggered fault slip on June 17, 2000 on the Reykjanes Peninsula, SW Iceland captured by radar interferometry. *Geophys. Res. Lett.* 30(6), 1273, doi:10.1029/2002GL015310.

Pedersen, R., F. Sigmundsson, K.L. Feigl and Þ. Árnadóttir 2001. Co-seismic interferograms of two Ms=6.6 earthquakes in the South Iceland Seismic Zone, June 2000. *Geophys. Res. Lett*. 28, 3341-3344.

Pedersen, R., S. Jónsson, Þ. Árnadóttir, F. Sigmundsson and K.L. Feigl 2003. Fault slip distribution of two Mw=6.5 earthquakes in South Iceland estimated from joint inversion of InSAR and GPS measurements. *Earth and Planetary Science Letters* 213, 487-502.

Rögnvaldsson, S.Th. and R. Slunga 1994. Single and joint fault plane solutions for microearthquakes in South Iceland. *Tectonophysics* 237, 73-86.

Slunga, R., S.Th. Rögnvaldsson and R. Böðvarsson 1995. Absolute and relative locations of similar events with application to microearthquakes in southern Iceland. *Geophys. J. Int*. 123, 409-419.

Stefánsson, R., G.B. Guðmundsson and P. Halldórsson 2003. The South Iceland earthquakes 2000 – a challenge for earthquake prediction research. *Icelandic Meteorological Office – Report* 03017.

Tryggvason, A., S.Th. Rögnvaldsson and Ó.G. Flóvenz 2002. Three-dimensional imaging of the P-and S-wave velocity structure and earthquake locations beneath southwest Iceland. *Geophys. J. Int*. 151, 848-866.

Vogfjörð, K.S., G. Nolet, W.J. Morgan, R.M. Allen, R. Slunga, B.H. Bergsson, P. Erlendsson, G. Foulger, S.S. Jakobsdóttir, B. Julian, M. Pritchard and S. Ragnarsson 2002. Crustal profiling in Iceland using earthquake source arrays. In: Abstracts from the AGU Fall Meeting, San Fransisco, California, December 6-10, 2002. Abstract S61C-1161.

Vogfjörð, K.S. 2003. Triggered seismicity in SW Iceland after the June 17, Mw=6.5 earthquake in the South Iceland Seismic Zone: The first five minutes. In: Abstracts from the EGS-AGU-EGU Joint Assembly, Nice, France, April 6-11, 2003. Geophysical Research Abstracts, vol. 5, 11251.

Weir, N.R.W., R.S. White, B. Brandsdóttir, P. Einarsson, H. Shimamura, H. Shiobara and the RISE Fieldwork Team 2001. Crustal structure of the northern Reykjanes Ridge and Reykjanes Peninsula, Southwest Iceland. *J. Geophys. Res*. 106, 6347-6368.

Wessel, P. and W.H.F. Smith 1991. Free software helps map and display data, *EOS Trans. Am. Geophys. Un.* 72, 441.